Crimson Publishers
Wings to the Research

Research Article

Preparation of Porous SiO_2-TiO_2-NiO Synthesized by the Sol-Gel Process and its Characterization

Chong-Santiago AJ[1], Mendoza-Serna R[1],*, Caballero-Díaz M[1], Valdez-Castro L[2] and Barrera-Cortés J[3]

[1]Career of Chemical Engineering, National Autonomous University of Mexico, Mexico

[2]Department of Engineering in Biotechnology, Polytechnic University of Puebla, Mexico

[3]Department of Biotechnology and Bioengineering, CINVESTAP-IPN, México

ISSN: 2576-8840

***Corresponding author:** Mendoza-Serna R, Career of Chemical Engineering, Zaragoza Experimental Research Multidisciplinary Unit (UMIEZ), Zaragoza School of Higher Studies, National Autonomous University of Mexico, Mexico

Submission: April 20, 2020

Published: May 11, 2020

Volume 13 - Issue 2

How to cite this article: Chong-Santiago AJ, Mendoza-Serna R, Caballero-Díaz M, et al. Preparation of Porous SiO_2-TiO_2-NiO Synthesized by the Sol-Gel Process and its Characterization. Res Dev Material Sci. 13(2). RDMS.000810. 2020.
DOI: 10.31031/RDMS.2020.13.000810

Abstract

An experimental strategy was developed to obtain Si-Ti-Ni transparent sols via the sol-gel process. The sol was prepared from $Si(OEt)_4$, $Ti(OBu)_4$ and Nickel(II) acetylacetonate. The chelating agent (2,4 pentanedione, acacH) was employed to stabilize Ti precursor in order to control their chemical reactivity, avoiding precipitation. A prehydrolyzed tetraethyl orthosilicate (TEOS) sol was the Si source. The sol was characterized by UV-Vis and Fourier Transform Infrared Spectroscopy (FTIR) spectroscopies. The solids treated were characterized by FTIR. Assignments of the simultaneous formation of the Si-O-Ti and Si-O-Ni bonds were done. The sol was polymerized at room temperature (293 K) to obtain gels and these were dried and treated at 673, 773 and 873 K in air. The characterization techniques were, X-ray Diffraction (XRD), Scanning Electron Microscopy (SEM), ^{29}Si Magic Angle Spinning Nuclear Magnetic Resonance (MAS NMR). The surface area of the solids was determined by N_2 adsorption/desorption isotherms. The corresponding average pore diameter was evaluated using the methods BJH, DA and HK. These models were used because all together cover the full range of the pore size. The purpose of producing porous polymeric system of SiO_2-TiO_2-NiO is to combine the properties of each of the oxides in a single material for use in catalytic reactions.

Keywords: Sol-Gel; SiO_2-TiO_2-NiO; Porous materials; Characterization techniques

Introduction

In recent decades, the synthesis and characterization of multi component materials has increased very rapidly [1]. The sol-gel method offers several advantages such as high purity of the final material, microstructure control, homogeneity on the molecular scale, and low-temperature preparation [2]. The goal of this research was to obtain porous SiO_2-TiO_2-NiO systems, based on a controlled hydrolysis-condensation process of the components. Silica nanomaterials have several important properties that make them a unique matrix for incorporating functional components [3]. Titanium dioxide is an attractive material in the field of photo catalysis and solar energy conservation, due to its chemical inertness, very good stability, compatibility with other materials, non-toxicity and environmentally-friendly nature [4].

The homogeneous incorporation of Ti into SiO_2 matrix is important to obtain materials that exhibit chemical, thermal, and mechanical stability. Nickel oxide (NiO) is a semitransparent p-type semiconducting material, due to its excellent chemical stability, magnetic and optical properties has a wide range of applications, such as eletrochromic display devices, UV photo-detector, chemical sensors, and dye-sensitized solar cells [5]. Recently, supported NiO nanoparticles or thin films were suggested to be reactive for oxidative catalytic reactions, and much attention has been paid to the NiO-based catalysis [6]. Nickel oxide is among the most inexpensive good anode coloring materials, exhibiting relatively strong electrochromic properties and excellent contrast [7]. The synthesis of sols and gels on the formation of NiO/SiO_2 had produced composites with a controlled microstructure [8]. Several comparative studies have shown that in simulated physiological solutions NiTi is more resistant to chemical breakdown than 316L stainless steel [9], NiTi alloys have been recognized as desirable

materials for bone implants because of their excellent corrosion, wear resistance, biocompatibility, mechanical properties, and high strength to weight ratio [10], one SiO_2 film coating on the surface of TiNi can reduce the release of Ni ion to the human body [11]. Ni-based catalysts, with or without metal promoters or modifiers, are extensively studied with the objective or replacing much more expensive noble metals. The catalytic properties of the Ni/TiO_2-SiO_2 system have been reported in the literature for CO_2 reformation from methane to synthesis gas [12]. Therefore, we consider that the synthesis and characterization of a porous and homogeneous SiO_2-TiO_2-NiO material has multiple potential applications.

Experimental

The Si sol precursor was prepared by the HCl two-step catalyzed hydrolysis and condensation of Tetraethoxysilane (TEOS, Sigma Aldrich CAS: 78-10-4, 98%). TEOS was dissolved in anhydrous ethanol (EtOH, Sigma Aldrich CAS: 64-17-5) at room temperature and then deionized H_2O (Sigma Aldrich CAS: 7732-18-5) and a 1M Hydrochloric acid solution (CAS: 7647-01-0) were added. This solution was labeled A2 sol. The A2 sol was stirred and heated at 333K for 90min obtaining a stock sol. The molar ratios TEOS:EtOH:H_2O:HCl were $1.0:3.8:1.0:7x10^{-4}$. In the second step, more H_2O and HCl were added, so the final molar ratios TEOS:EtOH:H_2O:HCl were $1.0:3.8:5.1:6x10^{-3}$, respectively. The A2 sol was aged 2h and then mixed with Aluminum silicate hydroxide ($Al_2Si_2O_5(OH)_4$, Kaolin, Sigma Aldrich CAS: 1332-58-7), used as a molecular sieve to eliminate most of the H_2O molecules. The stock sol was filtered and recovered [13,14]. A solution composed of acacH (Sigma Aldrich CAS: 123-54-6) in EtOH was added to a sol containing titanium tetrabutoxide ($Ti(OBu)_4$, Sigma Aldrich CAS-5593-70-4) dissolved in EtOH. The mol ratio acacH:Ti was 2:1. The A2 sol was added dropwise to the chelating Ti sol (addition time: three hours). Subsequently, the Ni precursor, Nickel(II) acetylacetonate (Sigma Aldrich CAS: 3264-82-2) dissolved in EtOH was added. The final molar ratios SiO_2:TiO_2:NiO were 90:8:2. All the reactions were performed at room temperature (298K). The sol was transparent and stable during the whole polymerization process.

Characterization techniques

A Perkin Elmer λ10 spectrophotometer was used to obtain the UV-Vis spectra in the 200-450nm region. Quartz cells were used and EtOH was the solvent.

The FTIR spectra of the sols were obtained using a Varian 640 IR spectrophotometer in the 4000-500cm^{-1} region. The FTIR study of xerogels and oxides calcined was performed in the 2000-500cm^{-1} region.

The X-ray diffractograms were obtained using D8 Bruker Advance equipment applying CuKα radiation (λ=1.5406Å) ranging from 5° to 70° to determine the possible crystalline structure of the treated samples.

The morphologies of the samples were observed by using a scanning electron microscope (JEOL, JSM 6510) operating at 20kV.

The analysis of the samples in regard to the temperature that the material supports was through the application of Thermogravimetry with a team brand Perkin Elmer, model TGA400, with software Pyris; calibrating the equipment with the metals Alumel, Perkalloy and Fierro and initiating the heating at 303K up to a temperature of 1173K and with a heating ramp of 10K/min, in a nitrogen atmosphere. Calorimetry Scanning Difference (DSC) was applied, with a Mettler Toledo equipment, Model DSC1, with STAR software version 14.0; calibrating the equipment with three methods: for temperature adjustment, heat flow and total calibration; and initiating the heating at 123K up to a temperature of 773K and with a heating ramp of 10K/min, in a nitrogen atmosphere.

The N_2 adsorption/desorption isotherms of the xerogels treated at 673, 773 and 873K, were measured at 77K in a Belsorp-mini II equipment with software version 2.4.0. The samples were degassed with Helium at 573K for 12 hrs. The specific area of solids were calculated applying the BET method in the region of the relative pressure of $0.05 < P/Po < 0.5$.

The acquisition of the ^{29}Si spectrum was carried out in a Jeol 600MHz Nuclear Magnetic Resonance spectrophotometer model ECZ600R, using the pulse sequence Single pulse. For this, about 60mg of the sample was packed in a 3.2mm diameter rotor. The spectrum of ^{29}Si was acquired at 298K, with a relaxation time of 5 seconds, a pulse of 90° (10μs), 1024 scans and rotating at 15KHz.

Results and Discussion

The UV-Vis of the Si-Ti-Ni sol is shown in Figure 1. The sunlight´s radiation of below 280nm is almost completely absorbed by the atmosphere. Therefore, the UV spectrum suggests that the sample can exhibit photocatalytic activity under atmospheric conditions [15]. The FTIR bands Assignment for Si-Ti-Ni sol (Figure 2) is given in Table 1. The CH_3 stretching of Si-O-CH_3 was found in the fresh sol at 1273cm^{-1} and disappeared after thermal treatment at 673K (not shown here), as we expected due to the combustion of the organic groups [16]. The band at 910-960cm^{-1} is due to the overlapping of vibrations of Si-OH, Si-O-Ti bonds [15] (932cm^{-1}) [17] and Si-O-Ni (960cm^{-1}) [18], this region widens as a result of heat treatment. The bands in the wave number range up 556cm^{-1} are attributed to the deformation vibration of Si-O groups containing SiO_4 tetrahedra [19].

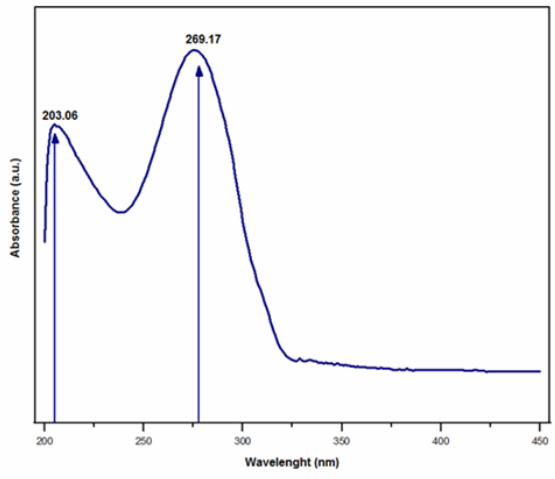

Figure 1: UV-Vis spectra of fresh Si-Ti-Ni sol.

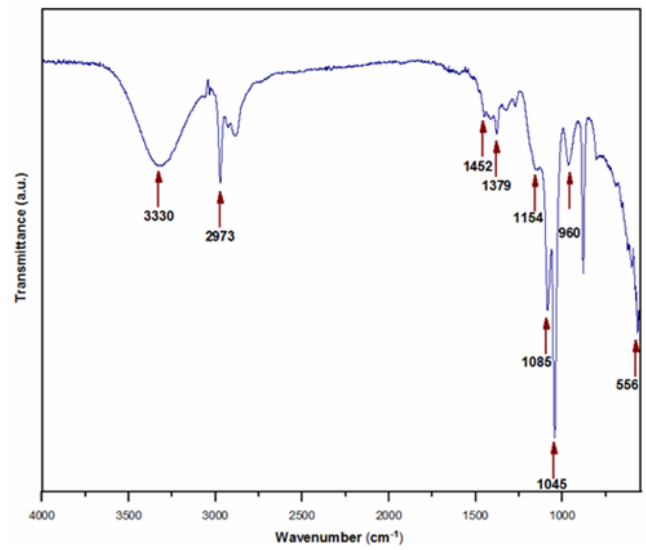

Figure 2: FTIR spectra of fresh Si-Ti-Ni sol.

Table 1: FTIR bands assignment in fresh Si-Ti-Ni sol.

Assignment	Wave Number (cm^{-1})
O-H stretching [27]	3330
C-H stretching [37]	2973
CH_3 bending [36]	1452
C-O-M stretching [39]	1379
O-H stretching in Si-OH [38]	1154
Si-O stretching in linear Si-O-Si [39]	1085
Si-O stretching in Si-O-Si disiloxane [39]	1045

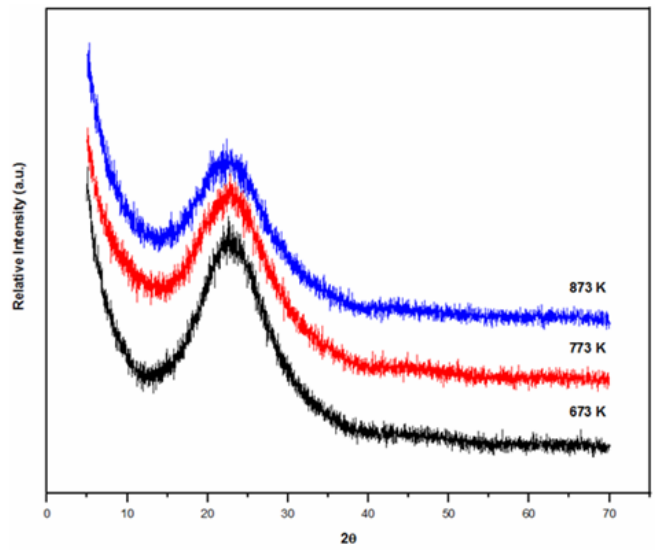

Figure 3: X-ray powder diffraction patterns at 673, 773 and 873K.

The Si-Ti-Ni powders analyzed by X-ray diffraction were found to be amorphous even at the temperature of 873K, Figure 3. The intense peak at 2Θ=22° indicates that the SiO_2 peak has amorphous nature [20]. No other impurity peaks were present in the Si-Ti-Ni powder. In X-ray diffraction patterns, the characteristic peaks of anatase 2Θ=25.6° (101), 38.17° (004), 48.3° (200) and 54.36° (105) is consistent with the values on the JCPDS card (No: 04-0477) [21] or rutile 2Θ=27.6° (110) [22], should not be observed for pure TiO_2 the transformation from anatase to rutile phase takes place at 873K. The three diffraction peaks are not observed at 2Θ=37.2° (111), 43° (200) and 63° (220) [23], which are identified as reflections of a cubic structure of NiO, respectively [24,25]. Additional peaks from NiO were not observed which signifies that NiO was incorporated into the structure of the SiO_2-TiO_2 [26].

The scanning electron microscopy images of Si-Ti-Ni treated at 673, 773 and 873K showed a trimodal size distribution, consisting of big, medium and small faceted particles. The SEM of 773 and 873K are presented in Figure 4a & 4b, respectively. The smaller particles of less 1μm, the medium 5μm and the larger ones are 20 and more μm. The morphology is well defined, showing different shapes, smooth and flat surfaces, faces and edges. The samples maintain the shape and sizes at 773 and 873K.

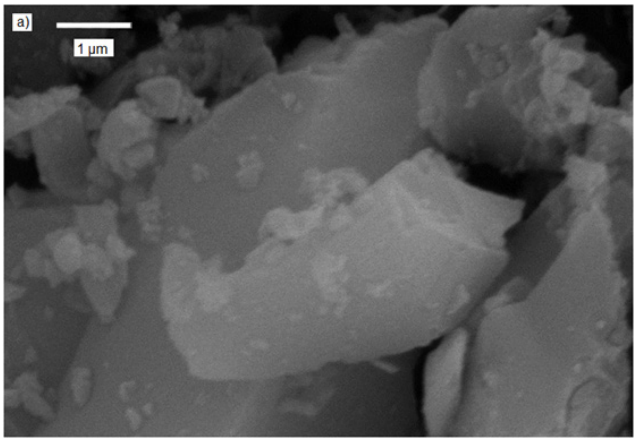

Figure 4(a): SEM photomicrograph of powders at 773K.

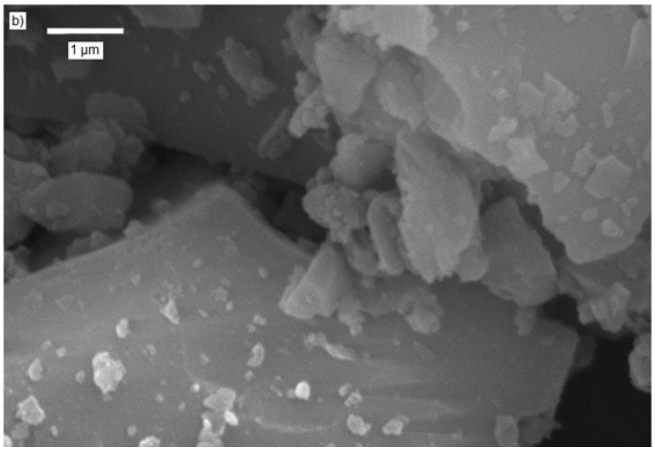

Figure 4(b): SEM photomicrograph of powders at 873K.

The materials synthesized were dried and later analyzed by thermal gravimetric analysis (TGA) and Differential Scanning Calorimetry (DSC). The TGA curve is shown in Figure 5. For a better description of the thermogravimetric study, it is divided into three temperature ranges.

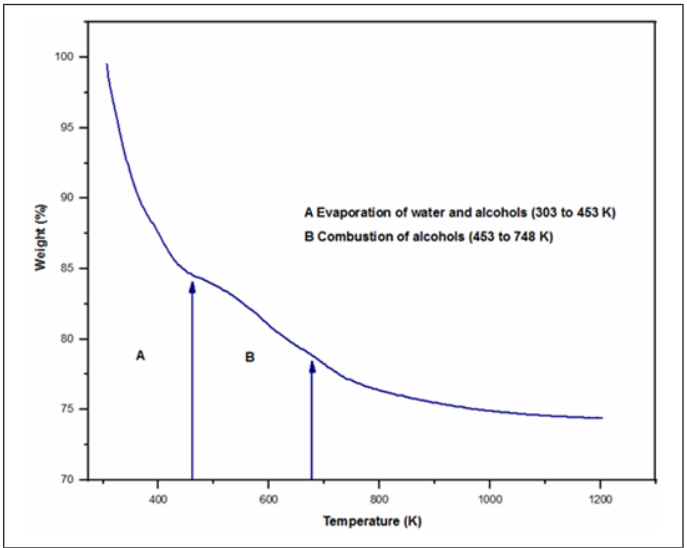

Figure 5: TGA curve of Si-Ti-Ni sample.

1. In the range of 303 to 453K, a greater weight loss is observed by evaporation of water and alcohols (ethanol and butanol) from silicon and titanium precursors (16%) [27]. Process that is justified by the endothermic peak at 365K present in the DSC (not shown here).

2. The second weight loss observed in the range of 453 to 748K associated to the combustion of alcohols (ethanol and butanol) as well as to groups ethoxide and peroxides of the condensation (7.5%) [28]. The DSC graph of this temperature range only shows one exothermic peak at 698K, which strengthens the aforementioned discussion.

3. Finally, in the temperature range 698 to 773K, a small weight change is observed, corresponding to the continuous dehydroxylation at high temperature of the formed material.

The isotherms for the samples at 673, 773 and 873K are shown in Figure 6. The first two samples exhibit a type I isotherm [29,30], indicating that micro porous material is present along with mesoporous one. The adsorbed volume gradually decrease between 673 and 773K, this temperature range correspond to the elimination of organic residue according the DSC graph. Sintering occurred during this calcining temperature range (773-873K). The sample treated at 873K exhibits characteristics of type IV isotherm that correspond to mesoporous materials [31]. The pore size distribution in the micro porous zone was evaluated using the method proposed by Dubinin-Astakhov (DA) [32], the pore size for the solids treated at 773 and 873K are shown in Figure 7. Horváth-Kawazo [33], the pore size distribution for the solid treated at 773K is shown in Figure 8. And for the solid treated at 873K in Figure 9. The pore size distribution in the mesopore zone was evaluated using the method proposed by Barret, Joiner and Halenda (BJH) [34]. The textural properties for the solids treated at 773 and 873K are shown in Table 2. There is a decrease in adsorbed volume and number of pores as a consequence of the heat treatment, even when at 873K the sintered material still has micropores. In the literature there are reported the calcined NiO at 873K embedded in silica matrix shows a slightly higher BET surface area, 450m^2/g, compared to that of the silica matrix itself, 400m^2/g, suggesting that the NiO contributed somehow to increase the adsorption capacity [3]. Others authors reported that the surface area and average pore size of their NiO/TiO_2/SiO_2 system treated at 773K were 265.3m^2/g and 12.6nm, respectively [6].

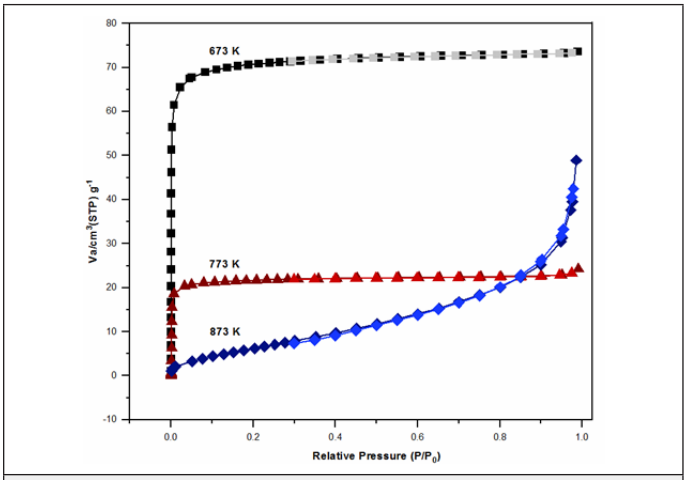

Figure 6: Nitrogen adsorption/desorption isotherms at: 673, 773 and 873K.

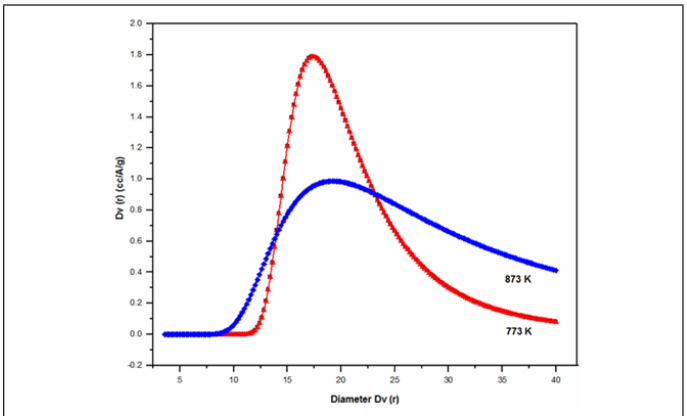

Figure 7: Pore size distribution at: 773 and 873K according to the Dubinin-Astakhov method.

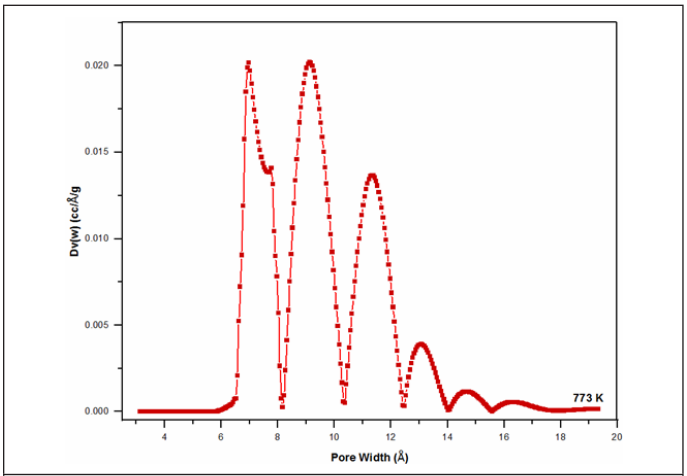

Figure 8: Pore size distribution of Si-Ti-Ni at 773K according to the Horváth-Kawazoe method.

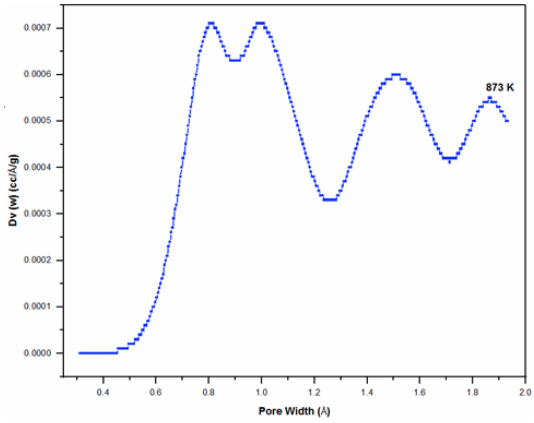

Figure 9: Pore size distribution of Si-Ti-Ni at 873K according to the Horváth-Kawazoe method.

Table 2: Porosimetry data of Si-Ti-Ni solids.

Sample	Temperature (K)	BET Surface Area (m^2/g)	Average Pore Diameter (nm) Method		
			BJH	DA	HK
Si-Ti-Ni	773	62.2	2.73	1.74	0.91
	873	28.2	3.40	1.92	0.99

The results for the ^{29}Si MAS NMR spectra of the Si-Ti-Ni solid sample calcined at 873K is observed in Figure 10. In order to compare the relative amounts of Q^1, Q^2, Q^3 and Q^4 species, we considered the chemical range -80 to -89.9ppm for Q1, -90 to -99ppm for Q^2, -99.1 to -108.9ppm for Q^3 and -109 to -120 for Q^4 [35]. The deconvolution with accuracy of 1% was 3.2 % Q^1, 13.0 % Q^2, 49.9 % Q^3 and 33.8 % of Q^4.

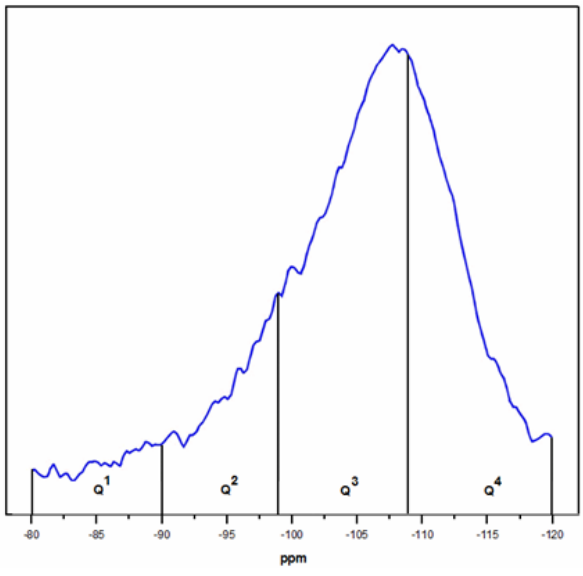

Figure 10: ^{29}Si MAS NMR spectra of Si-Ti-Ni treated at 873K.

Conclusion

The use of prehydrolysis of TEOS and the chelating agent acacH used to stabilize Ti ensure the homogeneity of the sols, gels, xerogels and oxides of SiO_2-TiO_2-NiO obtained up to 873K. The sample can exhibit photocatalytic activity under atmospheric conditions according to the UV-Vis results. The homogeneity of the material was demonstrated by FTIR with the presence of the characteristic bands of the Si-O-Ni and Si-O-Ti bonds and their stability with respect to thermal treatment, these results indicate that a homogeneous solid structure was produced. The powders analyzed by X-ray diffraction were found to be amorphous even after thermal treatment at 873K. The morphology analyzed by SEM shown that is well defined; the samples maintain the shape and sizes at 773 and 873K. A porous material was obtained that combine micro and mesoporous still at 873K. ^{29}Si MAS NMR indicate that the sample contain 50 % of specie Q^3.

Acknowledgement

A.J. Ch-S, R. M-S, M. C-D and L. V-C gratefully acknowledge DGAPA U.N.A.M. (Grant PAPIIT No. IN114516) for the funding for the fulfillment of this work.

References

1. Gary SS (1973) Fabrication of transparent electrooptic PLZT ceramics by atmosphere sintering. J Am Ceram Soc 56(2): 91-96.
2. Brinker CJ, Scherer GW (1990) Sol-Gel science, the physics and chemistry of Sol-Gel processing. Academic Press, San Diego, USA, pp. 839-841.
3. Mihaly M, Comanescu AF, Rogozea AE, Basile E, Meghea A (2011) NiO-silica based nanostructured materials obtained by microemulsion assiste sol-gel procedure. Mat Res Bull 46(10): 1746-1753.
4. Khojastech H, Salavati-Niasari M, Abbasi A, Azizi F, Enhessari M (2016) Synthesis, characterization and photocatalytic activity of PdO/TiO_2 and Pd/TiO_2 nanocomposites. J Mater Sci: Mater Electron 27: 1261-1269.
5. Wang N, Liu CQ, Wen B, Wang HL, Liu SM, et al. (2014) Enhance optical and electrical properties of NiO thin films prepared by rapid radiation pyrolysis method based on the sol-gel technique. Mat Lett 122: 269-272.
6. Eun JP, Ju HL, Kwang-Dae K, Dae HK, Myung-Geun J, et al. (2016) Toluene oxidation catalyzed by NiO/SiO_2 and NiO/TiO_2/SiO_2: Towards development of humidity-resistant catalysts. Catal Today 260: 100-106.
7. Ristova M, Velevska J, Ristov M (2002) Chemical bath deposition and electrochromic properties of NiOx films. Sol Ener Mat Sol C 71(2): 219-230.
8. Katsuhiko T, Tetsuhiko I, Mamoru S (1996) Effects of mechanical pretreatment of precursor sols and gels on the formation of NiO/SiO_2 composites with a controlled microstructure. J Non Cryst Solids 194: 58-62.
9. Duerig T, Pelton A, Stöckel D (1999) An overview of nitinol medical applications. J Mat Sci Eng A 273-275: 149-160.
10. Mohammad HE, Mahdi H, Majid T, Sarit BB (2012) Manufacturing and processing of NiTi implants: A review. Prog Mater Sci 57: 911-946.
11. Shu Y, Fei Z, Tao X, Da-bao X, Zhou L, et al. (2015) Surface modification with SiO_2 coating on biomedical TiNi shape memory alloy by sol-gel method. T Nonferr Metal Soc 25: 3723-3728.
12. Sanbing Z, Jiankang W, Xiaolai W (2008) Effect of calcinations temperature on structure and performance of Ni/TiO_2-SiO_2 catalyst for CO_2 reforming of methane. J Nat Gas Chem 17: 179-183.
13. Méndez-Vivar J, Mendoza-Serna R (1998) Sintering of SiO_2-TiO_2 Obtained by the sol-gel process from chelated Ti precursors. Scanning 20: 347-351.
14. Méndez-Vivar J, Mendoza-Serna R, Valdez-Castro L (2001) Control of the polymerization process of multicomponent (Si, Ti, Zr) sols using chelating agents. J Non Cryst Solids 288: 200-209.

15. Matavos-Aramyan S (2018) Preparation of Titania/Silica core-shell hybrid nanocomposites for 2014 Al-Alloy corrosion protection and investigation of their mechanical and thermal stability. Silicon 10: 1601-1612.

16. Méndez-Vivar J, Bosch P, Lara VH, Mendoza-Serna R (2002) Experimental design of Si-Ti-Zr polymers containing hybrid Si species, spectroscopy study and thermal evolution. J Porous Mat 9: 231-235.

17. Zhou L, Heinz H, Soucek MD, Alemán EA, Modarelli DA (2010) UV-Absorption and silica/titania colloids using a core-shell approach. Silicon 2: 95-104.

18. Saadi A, Lanasri K, Bachari K, Halliche D, Rabia Ch (2012) Catalytic reduction of benzaldehyde under hydrogen flow over nickel-containing mesoporous silica catalysts. Open J Phys Chem 2: 73-80.

19. Salinigopal MS, Gopakumar N, Anjana PS (2019) Alkaline earth based borosilicate glasses as sealants in solid oxide fuel cell applications. Silicon 12: 101-107.

20. Gholami T, Bazarganipour M, Salavati-Niasari M, Bagheri S (2015) Photocatalytic degradation of methylene blu on TiO_2@SiO_2 core/shell nanoparticles: synthesis and characterization. J Mater Sci: Mater Electron 26: 6170-6177.

21. Safajou H, Khojasteh H, Salavati-Niasari M, Mortazavi-Derazkola S (2017) Enhanced photocatalytic degradation of dyes over graphene/Pd/TiO_2 nanocomposites: TiO_2 nanowires versus TiO_2 nanoparticles. J Colloid Interface Sci 498: 423-432.

22. Wojcieszak D (2017) Analysis of Eu-effect on stabilization of the TiO_2-anatase structure in high temperature and photoluminescence efficiency for the coatings as-deposited in magnetron sputtering process. Appl Surf Sci 421: 128-133.

23. Sun H, Kuo TY, Chen ShC, Chen YH, Lin, et al. (2019) Contibution of enhanced ionization to the optoelectronic properties of p-type NiO films deposited by high power impulse magnetron sputtering. J Eur Ceram Soc 39: 5285-5291.

24. Sheng-Hui L, Fu-Rong Ch, Ji-Jung K (2008) Electrochromic properties of nano-structured nickel oxide thin film prepared by spray pyrolysis method. Appl Surf Sci 254(7): 2017-2022.

25. Mrabet C, Ben AM, Boukhachem A, Amlouk M, Manoubi T (2016) Physical properties of La-doped NiO sprayed thin films for optoelectric and sensor applications. Ceram Int 42(5): 5963-5978.

26. Mahnaz A, Nasrollah NI (2018) Effect of Ni doping on the structural optical properties of TiO_2 nanoparticles at various concentration and temperature. Silicon 10: 2569-2575.

27. Duran A, Serna C, Fornes V, Fernández Navarro JM (1986) Structural considerations about SiO_2 glasses prepared by sol-gel. J Non Cryst Solids 82: 69-77.

28. James PF (1988) The gel to glass transition: Chemical and microstructural evolution. J Non Cryst Solids 100: 93-114.

29. Lowell S, Shields JE (1991) Power surface area and porosity. Scarlett B (Ed.), (3rd edn), Chapman & Hall, UK, p. 72.

30. Gregg SJ, Sing KSW (1982) Adsorption, surface area and porosity. Academic Press London, UK, pp. 195-247.

31. Brunauer S, Deming LS, Deming WE, Teller E (1940) On a theory of the van der waals adsorption of gases. J Am Chem Soc 62: 1723-1732.

32. Dubinin MM, Astakhov VA (1971) Development of the concepts of volume filling of micropores in the adsorption of gases and vapors by microporous adsorbents. Bull Acad Sci USSR, Div Chem Sci 20: 3-7.

33. Horvát G, Kawazoe K (1983) Method for the calculation of effective pore size distribution in molecular sieve carbon. J Chem Eng Jpn 16: 470-475.

34. Barret EP, Joyner LG, Halenda PP (1951) The determination of pore volume and area distributions in porous substances. I Computations from Nitrogen Isotherms. J Am Chem Soc 73(7): 373-380.

35. Liu Z, Crumbaugh GM, Davis RJ (1996) Effect of structure and composition on epoxidation of hexene catalyzed by microporous and mesoporous Ti-Si mixed oxides. J Catal 159: 83-89.

36. Mendoza-Serna R, Méndez-Vivar J, Loyo-Arnaud E, Moreno-Rodríguez JA, Bosch P, et al. (2003) Preparation and characterization of porous SiO_2-Al_2O_3-ZrO_2 prepared by the sol-gel process. J Porous Mat 10: 31-39.

37. Nakamoto K (1997) Infrared and raman spectra of inorganic and coordination compound. John Wiley & Sons (Eds.), (5th edn), USA, p. 356.

38. Pouchert CJ (Ed.) (1981) The aldrich library of infrared spectra, (3rd edn), Aldrich Chemical, Milwaukee, USA, p. 246.

39. Pouchert CJ (Ed.) (1981) The aldrich library of infrared spectra, (3rd edn), Aldrich Chemical, Milwaukee, USA, p. 252.